International Journal of Heat and Mass Transfer 62 (2013) 435–444

Contents lists available at SciVerse ScienceDirect

International Journal of Heat and Mass Transfer

journal homepage: www.elsevier.com/locate/ijhmt

Multiscale modeling of thermoelectric generators for the optimized conversion performance

Siyi Zhou [a,*], Bahgat G Sammakia [a], Bruce White [b], Peter Borgesen [c]

[a] Department of Mechanical Engineering, Binghamton University-SUNY, Binghamton, NY 13902, United States
[b] Department of Physics, Applied Physics and Astronomy, Binghamton University-SUNY, Binghamton, NY 13902, United States
[c] Department of System Science and Industrial Engineering, Binghamton University-SUNY, Binghamton, NY 13902, United States

ARTICLE INFO

Article history:
Received 3 December 2012
Received in revised form 23 February 2013
Accepted 2 March 2013
Available online 9 April 2013

Keywords:
Micro scale
Conversion efficiency
Seebeck effect
Thermoelectric

ABSTRACT

An attractive option for constructing thermoelectric generators (TEGs) is to incorporate a water-fed heat exchanger with commercially available thermoelectric modules. In this paper, two different thermoelectric models are applied to predict the energy conversion performance of the TEGs. The first model employs a derivation of the Carnot efficiency. The second model presents a rigorous interfacial energy balance by capturing Joule heating, Seebeck, Peltier and Thomson effects, yielding better predictions of the conversion capability. This model is then used to perform a computational examination of the TEGs embedded in 30 different configurations, which allows the identification and quantification of key design parameters including flow types, hot stream inlet temperatures (T_{in_hot}), pressure drops (ΔP), cross-sectional area (A_C), channel length (L_{ch}) and number of channels. The positive effects of T_{in_hot} and ΔP can be easily captured and parallel flows of the hot and cold streams are found to provide greater overall TEG efficiency as compared to counter flows. In general, micro-sized A_C reduces temperature gradients across the channels, providing a greater ΔT across the thermoelectric material. However, enhancements of the conversion capability are eventually limited by the reduced convective heat transport due to increased flow resistance. Finally, further improvements in the power generation are achieved by reducing L_{ch} while increasing the number of channels. The resulting reduction in flow resistance is found to facilitate increases in convective heat transfer, as well as in ΔT, and thus a great increase in conversion efficiency (η).

1. Introduction

Thermoelectrics are in principle, attractive for the conversion of waste heat into electric power. The underlying mechanisms dictating thermoelectric effects were not well understood until the discovery of the electron at the end of the 19th century. It is now known that electrons, or holes, in a solid carry both charge and heat. When a temperature drop is applied across a thermoelectric material, as shown in Fig. 1, this will cause the net diffusion of electrons (holes) from the hot side to the cold side. The electrical potential produced by the temperature difference is known as the Seebeck effect, and devices that generate electrical power by virtue of the Seebeck effect are called thermoelectric generators (TEGs). Alternate electrical connections of the hot sides and cold sides of a series of n- and p-type materials allow the build-up of any desired voltage.

TEGs have great potential in the direct conversion of waste-heat energy from power plants and automotive vehicles into electric power where it is unnecessary to consider the cost of the thermal energy input, and offer reliable power in remote areas such as in space and at mountain top telecommunication sites [1]. Unlike traditional dynamic heat engines, TEGs present several distinct advantages over other technologies, such as being simple, compact and highly reliable, being capable of operating at elevated temperatures, being suited for small-scale and remote applications, and being environmentally friendly [2,3]. A major limitation is, however, the low conversion efficiency of current thermoelectric devices (typically around 5–10% [4]), which is mainly caused by the available thermoelectric materials in the direction of figure of merit and has restricted their use in specialized fields with extensive applications. Since the promotion of the intrinsic efficiencies of the TE materials at device level has yet to be proved, there are ongoing attempts to increase the competitiveness of TEGs by improving the way in which they are currently used, offering some significant guidelines for design optimization [5–7]. The maximum efficiency of TEGs is subject to the constraints of the second law of thermodynamics, with the limit being expressed as $\eta_{max} = \Delta T/T_h$,

* Corresponding author.
E-mail addresses: szhou3@binghamton.edu (S. Zhou), bahgat@binghamton.edu (B.G Sammakia), bwhite@binghamton.edu (B. White), pborgese@binghamton.edu (P. Borgesen).

0017-9310/$ - see front matter © 2013 Elsevier Ltd. All rights reserved.
http://dx.doi.org/10.1016/j.ijheatmasstransfer.2013.03.014

Nomenclature

x	axial distance along fluid flow axis, m
L	TEG length, m
W	TEG width, m
H	TEG height, m
P	pressure in flows, Pa
T	temperatures, K
C_p	specific heat capacity at constant pressure, J/kg K
N_u	Nusselt number
A	area, m^2
G	volume flow rate, m^3/s

Greek symbols

κ	thermal conductivity, W/K m
σ	electric conductivity of TE material, S/m
δ	Seebeck coefficient of TE material, V/K
ρ	density, kg/m^3

Subscripts

h, c	hot side and cold side of thermoelectric layer
TE	thermoelectric
ch	channel
avg	average
in_hot, in_cold	inlet of hot and cold stream
1–5	length number
$conv$	convection

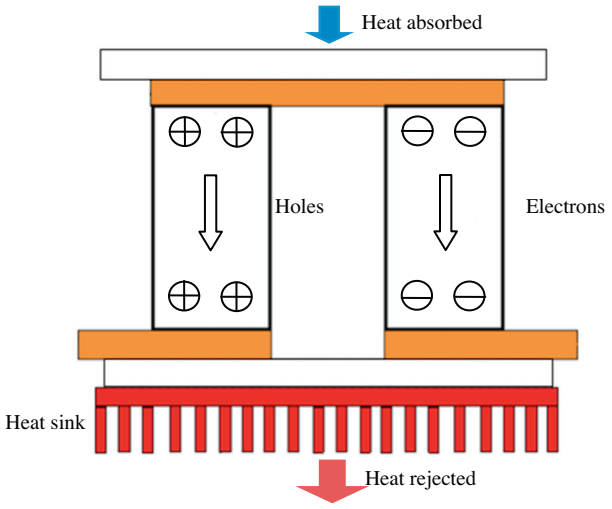

Fig. 1. Schematic illustration of a typical TEG. The construction consists of a pair of p-type and n-type semiconductor materials forming a thermocouple. Electron (Hole) diffusion is shown in this figure driven by a temperature difference.

where T_h is the temperature of the thermoelectric module hot side, and a principal focus has been on improving generator efficiency by maximizing the temperature drop (ΔT) across the thermoelectric modules. Traditional efforts have aimed to achieve this through the design of heat exchangers. Esarte et al. [8] theoretically addressed the optimization of heat exchanger geometries and various operating conditions including fluid flow rates, fluid properties and inlet temperatures. Crane et al. [9] investigated a computational model for the integration of a thermoelectric heat exchanger in a cross flow configuration. In the case of TEGs with large-scale multi-panels [10] and cylindrical multi-tubes [11], a mathematical expression for power output was deduced, considering different geometrical systems. Experiments have also been conducted on TEGs intended for low-temperature waste heat power recovery to assess effects of inlet temperature and flow rate on power output and conversion efficiency [12].

All of these research efforts combined thermoelectric modules with macro-scale heat exchangers, but growing applications such as autonomous micro-systems or wearable electronics look for micro-scale power generators. A micro TEG was proposed to provide electric power for an electronic chip in a domestic gas-monitoring system. In excess of 1.5 V could be produced when ΔT of a few tens of degrees was established [13]. Moreover, the utilization of TEGs in reciprocating internal combustion engines is another novel application. A comprehensive theoretical study of applying a TEG to automotive engine waste heat recovery is conducted [14]. By utilizing ΔT of 563 K between a micro-channel heat sink and exhaust gas, the maximum power of 51.13 mW/cm^2 can be reached.

Enormous amounts of research have been conducted on applications of TEGs. However, these thermoelectric systems are constrained by their low thermodynamic efficiencies, which means that a comparatively large amount of heat is required to produce a given quantity of electricity. Thus, there is a clear need for further improvements in the design of the heat exchangers as well as matching of the heat exchanger and thermoelectric designs. In this paper, the device performance of a water-fed heat exchanger based TEG in a range of scales is estimated by a simulation approach, which offers more detailed predictions than analytical methods, and can be more cost-effective than, or eventually help guide, experiments. The simulations are performed using the commercial FEA package COMSOL™ [15]. Two different thermoelectric models are applied in this paper. The first is the Simple model derived from the Carnot efficiency, and the second is the Coupled-field model presenting a rigorous interfacial energy balance by capturing Joule heating, Seebeck, Peltier, and Thomson effects.

Experiments conducted by Niu et al. [16] are employed here to demonstrate the applicability of the two thermoelectric models for evaluating TEGs device performance. The model showing the best agreement, by comparison with the experimental measurements, is used to perform a computational examination of TEGs embedded in 30 different configurations, which allows the identification and quantification of systematic effects of key design parameters including flow types (parallel flows & counter flows), hot stream inlet temperatures (T_{in_hot}), pressure drops (ΔP), cross-sectional area (A_C), channel length (L_{ch}) and number of channels. The positive effects of T_{in_hot} and ΔP on energy extraction are captured. Micro-scale A_C values provide smaller temperature gradients across the channels and thus a greater ΔT across the thermoelectric material. However, enhancements of the conversion capability are eventually limited by reduced convective heat transport due to increased flow resistance. Finally, further improvements in the power generation are achieved by reducing L_{ch} and increasing the number of channels.

2. Thermoelectric models

2.1. Simple model

In the Simple model established previously by the authors [17], the three-dimensional Navier–Stokes and energy equations combined with the continuity equation are solved simultaneously to

determine the temperature fields across the thermoelectric module.

The governing equations read as follows,

Continuity equation:

$$\nabla \cdot (\rho \mathbf{u}) = 0 \tag{1}$$

Momentum conservation equation:

$$\rho(\mathbf{u} \cdot \nabla \mathbf{u}) = -\nabla P + \nabla \cdot \varphi + \mathbf{F} \tag{2}$$

Energy equation:

$$\mathbf{u} \cdot \nabla T = \frac{\kappa}{\rho C_P} \nabla^2 T + \frac{\dot{Q}}{\rho C_P} + \frac{S}{\rho C_P} \tag{3}$$

where $\mathbf{F}$ represents body forces acting on the fluid, φ is the stress tensor, S is the dissipation function due to the viscous force, and $\dot{Q}$ is the rate of internal heat generation within the solid domain. The energy equation is solved in the fluid and solid domains where the heat transfer is strictly by convection and conduction respectively. For the fluid domain, $\dot{Q}$ is zero; for the solid domain, the convective term and S are zero, while $\dot{Q} = -W'$. W' is the electric power extracted by the TEGs and can be expressed as,

$$dW' = \eta_{\max} dq \tag{4}$$

q is the heat flow rate by conduction across the thermoelectric layer, which may be evaluated from Fourier's law,

$$dq = -\kappa_{\mathrm{TE}} dydz \frac{\partial T}{\partial x} - \kappa_{\mathrm{TE}} dxdy \frac{\partial T}{\partial z} - \kappa_{\mathrm{TE}} dxdz \frac{\partial T}{\partial y} \tag{5}$$

Limited by the second-law of thermodynamics, the ideal efficiency of a TEG operating as a reversible heat engine is Carnot efficiency, given by

$$\eta_{\mathrm{Carnot}} = 1 - \frac{T_c}{T_h} \tag{6}$$

The maximum conversion efficiency of an irreversible TEG can be estimated by [18]

$$\eta_{\max} = \eta_{\mathrm{Carnot}} \left[\frac{\sqrt{1 + Z\frac{T_h + T_c}{2}} - 1}{\sqrt{1 + Z\frac{T_h + T_c}{2}} + \frac{T_c}{T_h}} \right] \tag{7}$$

The figure of merit Z for the thermoelectric devices can be defined as,

$$Z = \frac{\delta^2 \sigma}{\kappa_{\mathrm{TE}}} \tag{8}$$

In general, a TEG exhibits low efficiency due to the relatively small, dimensionless figure-of-merit ($Z\overline{T}$, a metric of measuring currently available thermoelectric materials' performance at a particular temperature). By solving Eqs. (1)–(8) simultaneously, the temperature profiles of thermoelectric layers are first obtained and substituted into Eq. (4) to get the value of W'. This value is then coupled back to Eqs. (1)–(8) to get the updated temperature field, and the power W'.

2.2. Coupled-field model

While the Simple model has being frequently used to estimate the potential performance of thermoelectric devices, the diversity and complexity of thermoelectric applications necessitate a fully Coupled-field model, which, in addition to Joule heating, accounts for Seebeck, Peltier and Thomson effects as coupling mechanisms between thermal and electric fields. The equations governing the multidimensional temperature and electrical potential distributions in the TEGs under steady-state conditions and in the absence of an applied magnetic field are shown as,

Momentum conservation equation reads,

$$\rho(\mathbf{u} \cdot \nabla \mathbf{u}) = -\nabla P + \nabla \cdot \varphi + \mathbf{F} \tag{9}$$

Energy conservation for the liquid domain shows,

$$\mathbf{u} \cdot \nabla T = \frac{\kappa}{\rho C_P} \nabla^2 T + \frac{S}{\rho C_P} \tag{10}$$

Energy conservation for the solid domain involves Joule heating,

$$\nabla(\kappa_{\mathrm{TE}} \cdot \nabla T) - T \cdot \mathbf{J} \cdot \left(\frac{\partial \delta}{\partial T} \right) \cdot T + \rho_{\mathrm{TE}} \cdot \mathbf{J} = 0 \tag{11}$$

In this model, the equations of heat flow Eq. (11) and of continuity of electric charge [19] Eq. (12) are coupled by the set of thermoelectric constitutive equations, Eqs. (13) and (14).

$$\nabla \cdot \mathbf{J} = 0 \tag{12}$$

$$\mathbf{q} = [\Pi] \cdot \mathbf{J} - [\kappa] \cdot \nabla T \tag{13}$$

$$\mathbf{J} = [\sigma] \cdot (\mathbf{E} - [\delta] \cdot \nabla T) \tag{14}$$

where, $\mathbf{q}$ is the heat flux vector, $\mathbf{J}$ is the electric current density vector, $\mathbf{E}$ is the electric field intensity, $[\kappa]$ is the thermal conductivity matrix, $[\sigma]$ is the electrical conductivity matrix, $[\delta]$ is the Seebeck coefficient matrix, $[\Pi] = T[\delta]$ is the Peltier coefficient matrix. In the absence of time-varying magnetic fields, $\mathbf{E}$ is irrotational, and can be derived from an electric scalar potential φ,

$$\mathbf{E} = -\nabla \varphi \tag{15}$$

The flow field needs to be incorporated into the thermoelectric schemes, which requires the addition of Navier–Stokes model. The equations governing weakly compressible Navier–Stokes Flow can be found in Eqs. (1)–(3).

Therefore, the electric power W' can be calculated as

$$W' = \frac{V_{\mathrm{OC}}^2}{2(R_{\mathrm{TE}} + R_{load})} \tag{16}$$

where, V_{OC} is the open circuit voltage, R_{TE} is the internal thermoelectric resistance, and R_{load} is the electric resistance of the external load. For the maximum electrical power, $R_{load} = R_{\mathrm{TE}}$.

2.3. Conversion efficiency

A term η is referred to as the overall TEG efficiency and can be defined as,

$$\eta = \frac{W'}{Q_h} = \frac{W'}{\oint_{A_{inlet} - A_{outlet}} \rho C_P \mathbf{u} T dA} \tag{17}$$

3. Solution procedure

3.1. Model evaluation

While the simulation is a common engineering practice, the validity of the proposed methodology becomes very important. The experiments conducted by Niu et al. [16] are used to demonstrate the applicability of each thermoelectric model for conversion capability prediction. The variations of power generation with T_{in_hot} from both simulations and experiments are shown in Fig. 2. The maximum power output obtained using the Simple model is approximately 30% higher than that of the experiment, which may due to the electric field is not considered in this model. The comparison between model predictions and experiments clearly indicates that the Coupled-field model shows better performance as compared to the Simple model, which is then used in the succeeding simulations to examine the key design parameters for TEGs.

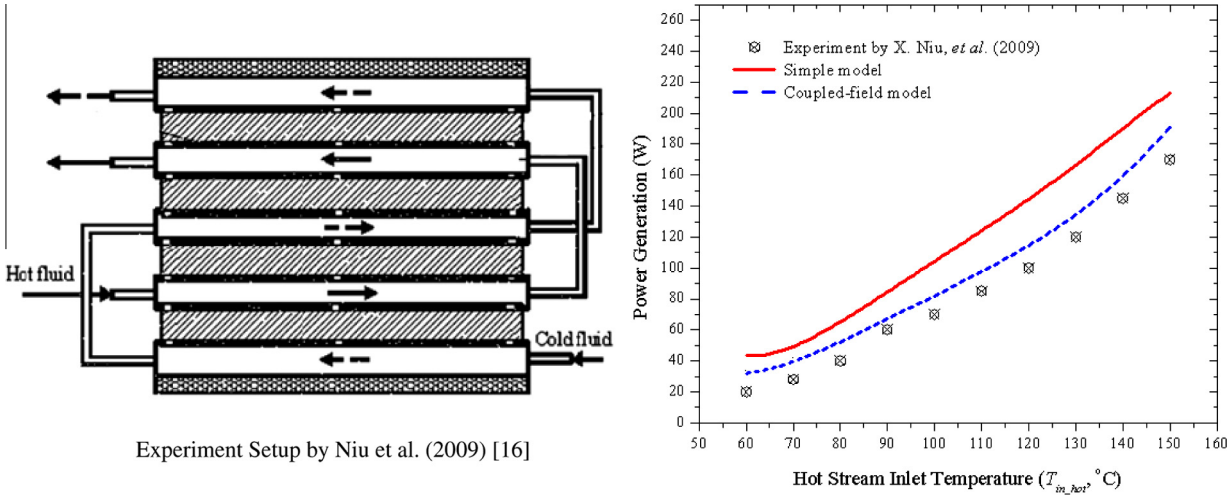

Fig. 2. Model validations with maximum power output at the reference conditions (T_{in_cold} = 293 K, G_{in_hot} = 0.4 m^3/h, G_{in_cold} = 0.3 m^3/h).

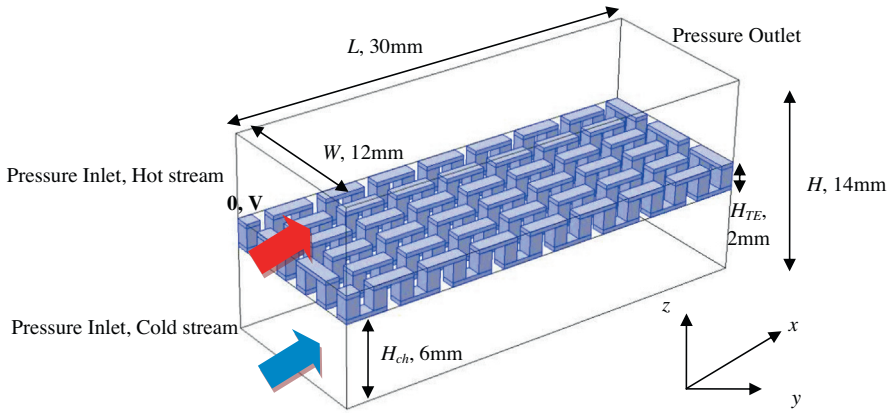

Fig. 3. Schematic layout of the proposed TEG considered in this study with boundary specifications.

3.2. Simulation specification

In this study, considering a basic TEG, an entire thermoelectric system of width, height and length ~W 12 mm by H 14 mm by L 30 mm is modeled consisting of a water-fed heat exchanger and commercially available thermoelectric modules. The numerical heat exchanger model is integrated with models for thermoelectric modules, which are positioned between hot and cold flow streams as shown in the schematic of a TEG section in Fig. 3. The heat applied from a hot stream is injected at the top of a thermoelectric layer and extracted by a cold stream at the bottom. The Seebeck effect can therefore generate electric power from ΔT across the thermoelectric layer. All subsequent thermoelectric schemes here are analyzed based on the Coupled-field model at a steady state operation, utilizing the commercial FEA package COMSOL™ through the Physics Interface Builder. The fluid flow in this study is along the x-axis shown in Fig. 3, and is assumed to be incompressible. The continuum assumption is accepted for the fluid studied here, as it is liquid water. The no-slip and no flow-through boundary conditions on all fluid/solid interfaces are invoked. Hot water enters inlet ports at 373 K, while cold water enters at 293 K. Wall thicknesses are neglected. There is natural air convection from all external surfaces, and the rate of heat transferred to the surrounding by convection is calculated by,

$$\dot{Q} = h_{conv} \cdot A_{conv} \cdot (T_s - T_\infty) \tag{18}$$

where h_{conv} is the convective heat transfer coefficient, A_{conv} is the area where convective heat transfer occurs, T_s is the surface temperature, T_∞ is the ambient temperature.

Different numbers of grid cells are used to perform a grid sensitivity study at the reference conditions (T_{in_cold} = 293 K, T_{in_hot} = 373 K, and ΔP = 2 bar). As shown in Fig. 4, a hexahedral mesh with at least a Degree of Freedom (DOF) of 700,000 is necessary to obtain a grid-independent result.

3.3. Thermoelectric material characterization

The thermoelectric material is a fundamental component of a TEG. Recent advances in materials and materials processing as summarized in recent reviews [20,21] have led to higher $Z\overline{T}$ values, and thus, higher theoretical η_{max}. For ΔT > 600 K, new thermoelectric materials i.e. Zn_4Sb_3-based compounds have exhibited η_{max} near 15% or more for ΔT > 800 K [22]. However, Bi_2Te_3-based compounds offer the best performance for T_h in a range of 350–400 K [23] where inexpensive fluids such as water can be used. These materials are taken as the focus of the current study, but our conclusions are more generally applicable. The thermoelectric leg in the simulations shown in Fig. 3 is 1 mm by 1 mm by 1.4 mm, capped by thin copper electrodes with the height of 0.3 mm. The material properties are tabulated in Table 1. Usually these are temperature-dependent and may be anisotropic, but we take them to be isotropic and constant.

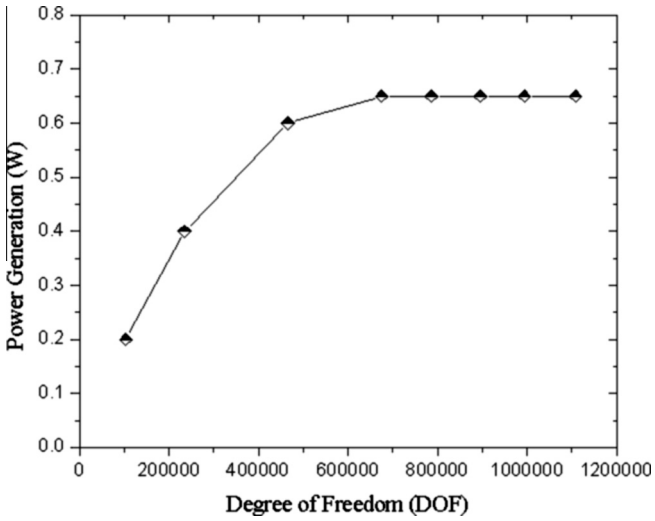

Fig. 4. Power generation for the case depicted in Fig. 3 vs. grid size using the Coupled-field model at the reference conditions (T_{in_cold} = 293 K, T_{in_hot} = 373 K, and ΔP = 2 bar).

Table 1
Material properties for TE modules.

	Symbol	Bi_2Te_3	Electrode (Copper)
Seebeck coefficient	δ, V/K	p: 2.2×10^{-4} n: -2.2×10^{-4}	6.5×10^{-6}
Thermal conductivity	κ, W/(K m)	1.5	350
Electric conductivity	σ, S/m	1.0×10^{5}	5.9×10^{8}
Density	ρ, kg/m^3	7740	8920
Heat capacity	Cp, J/(kg K)	154.4	385

4. Results and discussion

For the first calculation, the temperature profile of the baseline TEG depicted in Fig. 3 is shown in Fig. 5(a), while the voltage profile generated based on the Coupled-field model is indicated in Fig. 5(b). An electrical power of 0.65 W is obtained. As might be expected, an optimal heat exchanger for power generation would maximize ΔT across the thermoelectric layer by having minimal heat transfer resistance and, thus, minimum temperature drops at both the hot and cold side solid–liquid interfaces, as well as minimum temperature gradients across the height of the channels. In the following sections, the key design criteria are carefully examined.

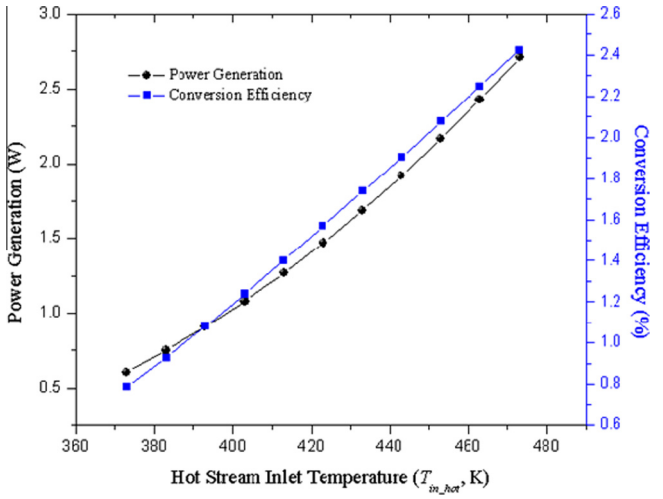

Fig. 6. Variation of the power generation and conversion efficiency with T_{in_hot} (T_{in_cold} = 293 K and ΔP = 2 bar).

4.1. Effect of hot stream inlet temperature (T_{in_hot})

Fig. 6 shows the increase in power generation and conversion efficiency with increasing the inlet temperature of the hot liquid, T_{in_hot}, assuming everything else (notably the cold inlet temperature) is kept constant. An increase in T_{in_hot} has two counteracting effects as far as η is concerned (according to Eq. (17)), but the increase in ΔT dominates that and the overall power generation increases faster than linearly. Not surprisingly, it is thus desirable to have the hot water delivered at as high a temperature as possible. Lowering the temperature of the cold liquid would have an even stronger effect on η, but that is not as often practical.

4.2. Effect of flow type and pressure drop (ΔP)

Simulations are carried out for both parallel flow (hot and cold flows in the same direction) and counter flow (hot and cold flows in the opposite direction) within the heat exchanger. Fig. 7(a) compares the variation of ΔT with flow distance from the inlet plane for parallel flow and counter flow, with a channel length of 2 m. For given inlet temperatures of each fluid, there is a significant

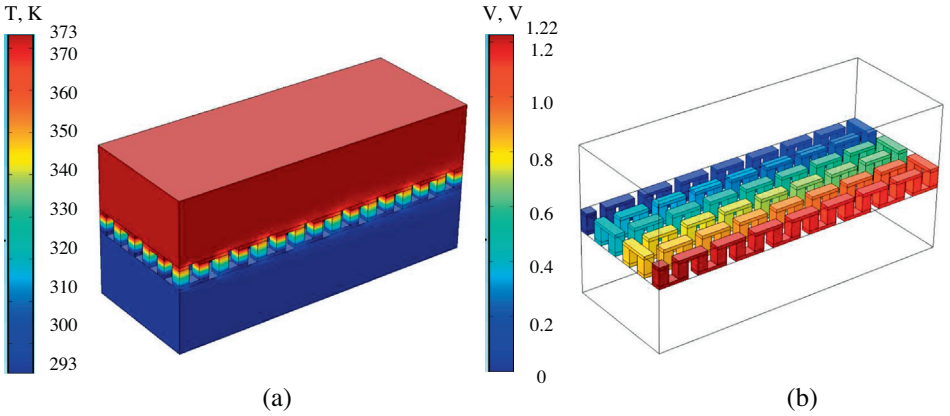

Fig. 5. (a) Temperature profile of the water-fed TEG at the reference conditions (T_{in_cold} = 293 K, T_{in_hot} = 373 K, and ΔP = 2 bar); (b) Voltage profile generated from the water-fed TEG based on the Coupled-field model.

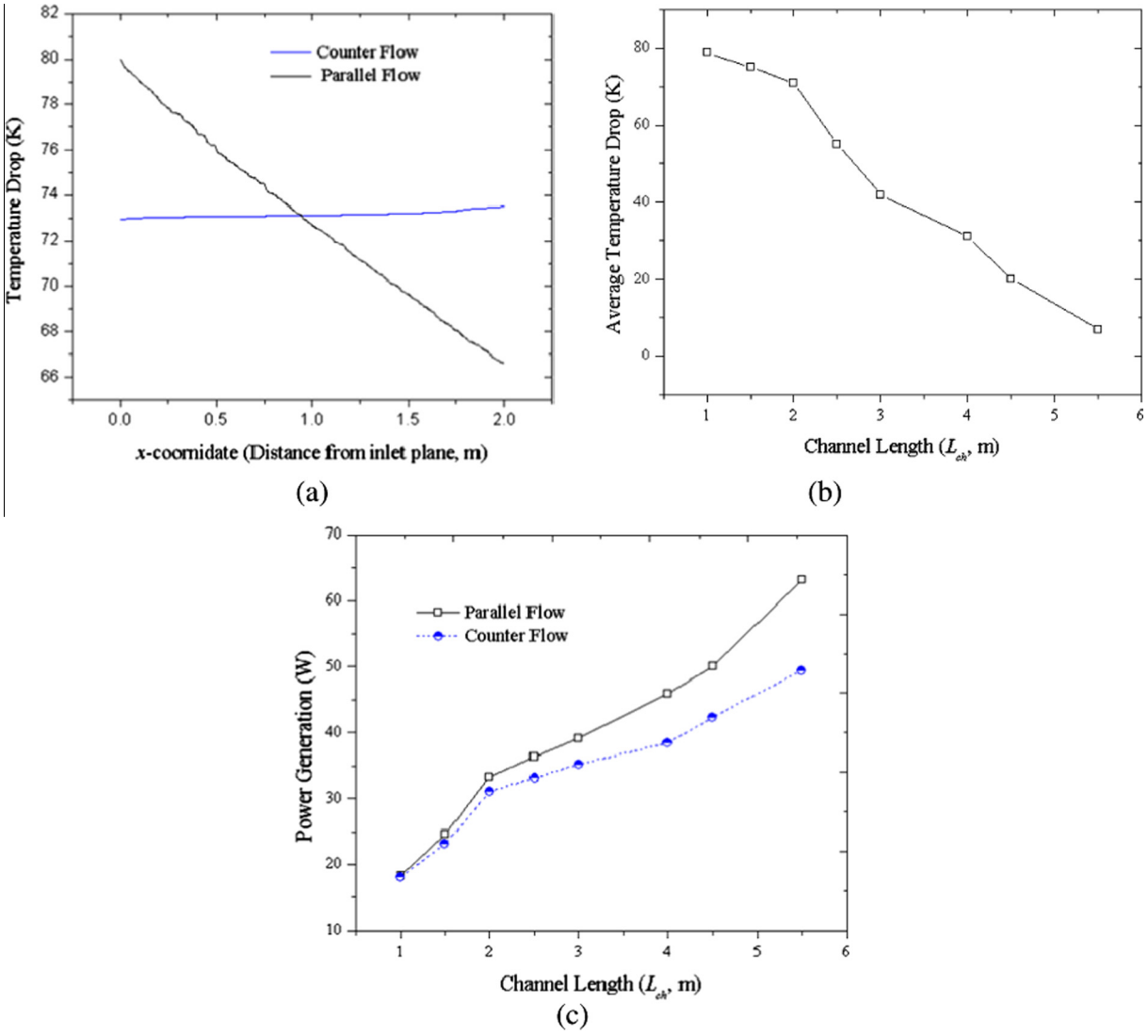

Fig. 7. Variation of (a) the temperature drop with flow distance from the inlet plane (L_{ch} = 2 m); (b) the average temperature drop between two fluids at the channel ends with L_{ch}; (c) power generation with L_{ch} for parallel flow vs. counter flow at the reference conditions (T_{in_cold} = 293 K, T_{in_hot} = 373 K, and ΔP = 2 bar).

variation in ΔT for parallel flow but a relatively smaller variation for counter flow. The average ΔT is basically the same for the two flow types, but η increases more than linearly with ΔT (Fig. 6) so we would expect the parallel flow to offer more electric power. We predict power generation of 33.5 and 32.2 W for parallel and counter flow, respectively, i.e. the flow type does not have a significant effect because ΔT only varies in a small range (where η increases linearly with ΔT). It becomes prominent in cases where the channel length is optimized, and has a larger ΔT. If a channel of optimized length can be reached, as well as a greater cooling along it, the effect of flow types becomes more prominent. Fig. 7(b) captures ΔT between the two fluids at the channel ends as a function of L_{ch} which increases from 1 to 5.5 m for the parallel flow. L_{ch} = 5.5 m is found to be optimum, since ΔT approaches to 0 K at the reference conditions (T_{in_cold} = 293 K, T_{in_hot} = 373 K, and ΔP = 2 bar) and there is no more available thermal energy to be converted. Variation of power generation with L_{ch} can be seen in Fig. 7(c). As expected, as L_{ch} increases, the parallel flow outperforms the counter flow.

Another important factor is the pressure drop, ΔP, which influences both the power output and the net power. The net power supplied by the TEG will be the total power output minus the power consumed by the pump driving the fluid through it, i.e.

$$W_{net} = W' - W_{PP} \tag{19a}$$

where

$$W_{PP} = \dot{V} \cdot \Delta P \tag{19b}$$

is the pumping power, ΔP is the pressure drop, and $\dot{V}$ is the volumetric flow rate. It is known that the convective heat transfer coefficient is changed by varying the fluid flow rate, which is increased by increasing ΔP through the channels of the heat exchanger. This leads to a variation in the thermal resistances of the heat exchanger, resulting in increases of ΔT and the power output.

Fig. 8 displays the total power output and the net electric power as a function of ΔP with everything else held constant. As ΔP increases, the total power output increases too, first relatively quickly and then leveling off. The net electric power, on the other hand, drops increasingly. This would seem to favor low values of ΔP, but not so low that the flow changes from turbulent to laminar (see below). Therefore, ΔP along the channel needs to be carefully considered for the TEGs design, and is kept constant at 2 bar in this

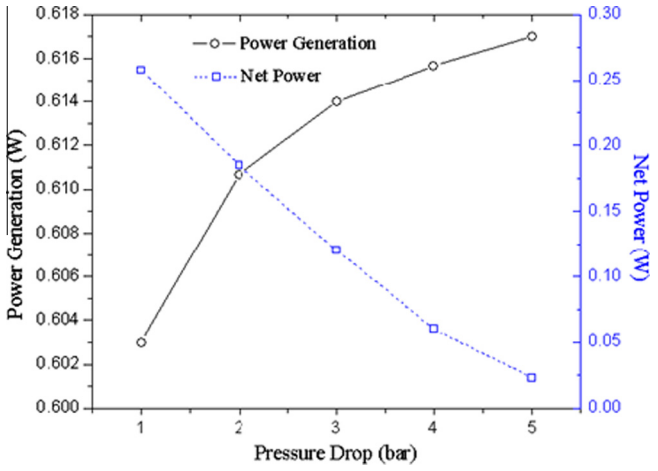

Fig. 8. Variation of the power generation and net power with pressure drop at the reference conditions (T_{in_cold} = 293 K, T_{in_hot} = 373 K, and parallel flow).

study, which also eliminates issues with phase change during the heat transfer process.

4.3. Effect of cross-sectional area (A_C)

Next, variations in the design of liquid channels and thermoelectric modules are assessed for fixed, outside heat exchanger dimensions (H 14 mm, W 12 mm, L 30 mm). For this purpose, the effects of the cross-sectional area of a single channel A_C are evaluated, assuming the same width W, length L, and fixed operation conditions. Distinction of different TEGs studied is based solely on the channel (thermoelectric module) height, H_{ch} (H_{TE}), in the z direction (Fig. 3). In essence, the baseline TEG in Fig. 3 consists of thermoelectric modules H_{TE} = 2 mm laminated between a hot (top) and a cold (bottom) channel, each of height H_{ch} = 6 mm, operating at a specific total pressure drop ΔP = 2 bar. As seen in Fig. 9, the next TEG (Case 2) consists of four hot channels and four cold channels assigned alternately (H_{ch} = 1.5 mm), with seven layers of thermoelectric modules (H_{ch} = 0.29 mm) sandwiched in between, meeting the same pressure drop constraint as the baseline TEG. This iteration is repeated for sequentially smaller distinct channels, as well as thermoelectric modules, as illustrated in Table 2. Eight levels of mesh resolution are tested to check the dependence of the solutions on grid design for each case in this study. Considering

Table 2
Different TEGs studied for A_C effect.

Case	# of channels	H_{ch} (mm)	H_{TE} (mm)
1	2	6	2
2	8	1.5	0.29
3	16	0.75	0.13
4	32	0.35	0.06
5	64	0.1875	0.03
6	128	0.09375	0.016

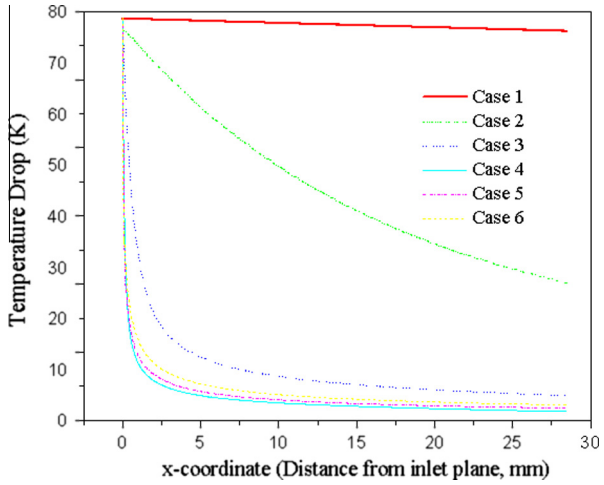

Fig. 10. ΔT across the thermoelectric modules along the flow direction are plotted for the TEGs in the six cases.

the balance between computational efficiency and the accuracy of results, suitable grid levels of resolution are chosen.

Fig. 10 shows the variation of ΔT across the thermoelectric layers with respect to the flow distance for the different cases, indicating the systematic effects of size as A_C moves from the macro-scale to the micro-scale. For Cases 1–3, ΔT remains significant until the end of the channel (30 mm), but less heat passes through without contributing to power generation as A_C decreases. The flow distance after which ΔT is essentially small, then increases again from an estimated 1.25 mm for Case 4, through 3.5 mm for Case 5 to 7.5 mm for Case 6.

As expected, the increase in effective heat transfer area at the interfaces between channels and thermoelectric layers, and the

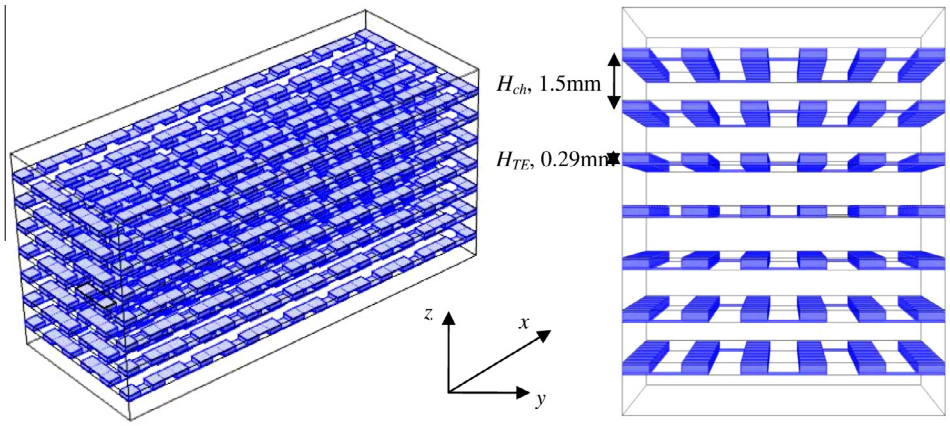

Fig. 9. Isometric view (a) and inlet (-x) view (b) of Case 2 is shown in this figure for A_C effect.

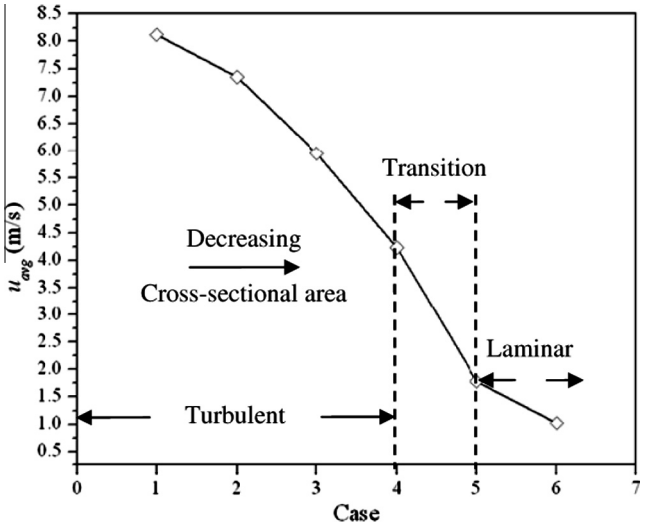

Fig. 11. u_{avg} at outlet port as a function of A_C; As A_C decreases, the trendline with three different slopes indicates three flow regions, i.e. turbulent, transition and laminar.

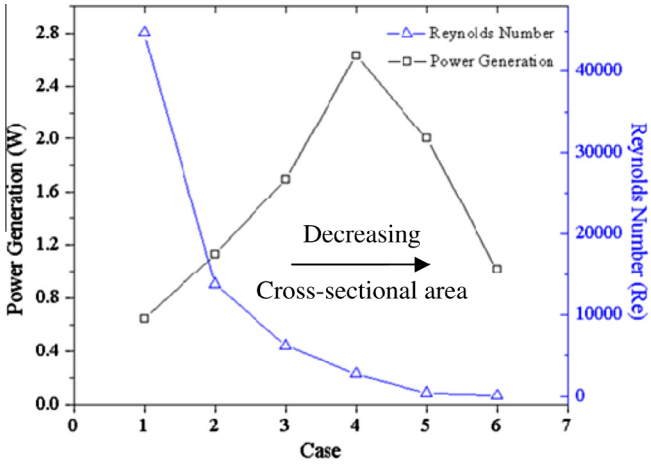

Fig. 12. Total power generated by the TEGs and *Re* with respect to A_C for the TEGs in the six cases at T_{in_cold} = 293 K, T_{in_hot} = 373 K, and ΔP = 2 bar.

reduction in individual layer thicknesses as the number of channels and thermoelectric layers increase tend to accelerate the heat transfer across the TEGs. However, the average velocity of water flow (u_{avg}) in the channels is lowered, since it is directly related to *Nu*. This reduces the equilibration of temperature across the

Table 3
Dimension specifications for all the five lengths.

	L (mm)	# of parallel unit
L_{ch1}	30	1
L_{ch2}	7.5	4
L_{ch3}	5	6
L_{ch4}	2.5	12
L_{ch5}		
Case 1	2.1	14
Case 2	1.6	19
Case 3	1.07	28
Case 4	0.8	38
Case 5	0.5	57
Case 6	0.5	57

height of a channel and thus has a negative effect on the heat transfer. Indeed, as the channels are getting sequentially smaller, ΔT across the individual thermoelectric layer decreases more quickly along the channel; this is not the case in Fig. 10. In fact, moving from Cases 4 to 6, u_{avg} drops precipitously as the reduction in channel height drives the water from turbulent flow to laminar flow (Fig. 11), and ΔT remains high for longer in spite of the fact that the effective heat transfer area keeps increasing.

Fig. 12 shows the total power generation for the six cases. The corresponding flow pattern is represented by the Reynolds number (*Re*) shown on the secondary axis (right). The conversion capability is shown to increase from Cases 1 to 4 because of the increased effective area for heat transfer together with a uniform temperature distribution across the height of the channel caused by the turbulent flow. This means that less heat is lost by passing through to the end of the channel, and a larger fraction of the heat is transferred to the thermoelectric layer while ΔT, and thus η is higher. Moving from Cases 4 to 6, however, the hydraulic diameter decreases enough for the flow to become laminar (reflected in *Re*) because of the increased flow resistance. The conversion capability is thus lowered for Cases 5 and 6, even though the effective area keeps increasing. We conclude that the optimal channel height is located at the onset of the transition from turbulent to laminar flow, as approximated in Case 4, and determined by the competition between this (u_{avg}) and the cross sectional area per channel, A_C.

4.4. Effect of channel length (L_{ch}) & number

The different effective distances along which ΔT across the thermoelectric layers is still relatively large in our calculations above show that none of the TEG designs considered are truly optimal. This can be clearly seen in Fig. 10, particularly for Cases 3–6 where ΔT across the TEGs are relatively low after x = 5 mm. The

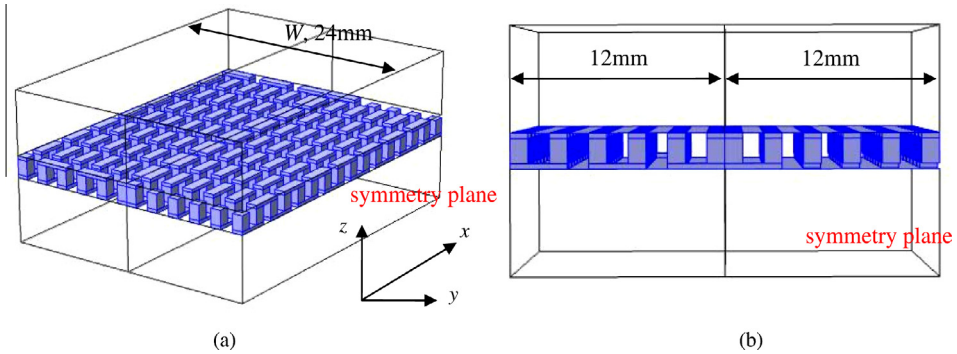

Fig. 13. Geometry specifications of Case 1 in L_{ch2} at isometric view (left) and inlet (-*x*) view (right). Hot and cold channels are isolated by thermoelectric modules.

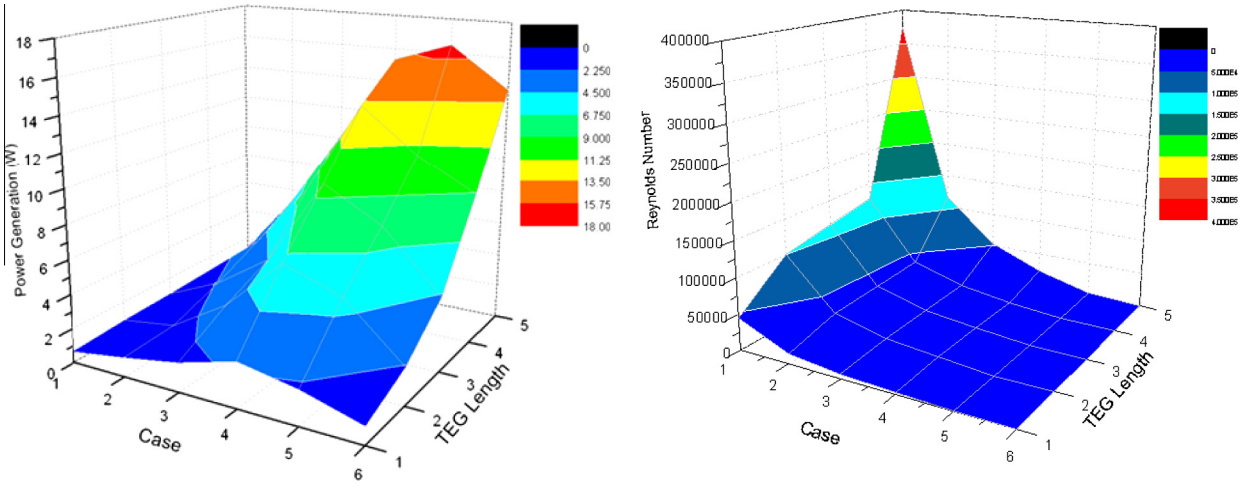

Fig. 14. (a) Power generated by the TEGs for L_{ch1}–L_{ch5} as a function of A_C at T_{in_cold} = 293 K, T_{in_hot} = 373 K and ΔP = 2 bar. (b) *Re* of the TEGs for L_{ch1}–L_{ch5} as a function of A_C.

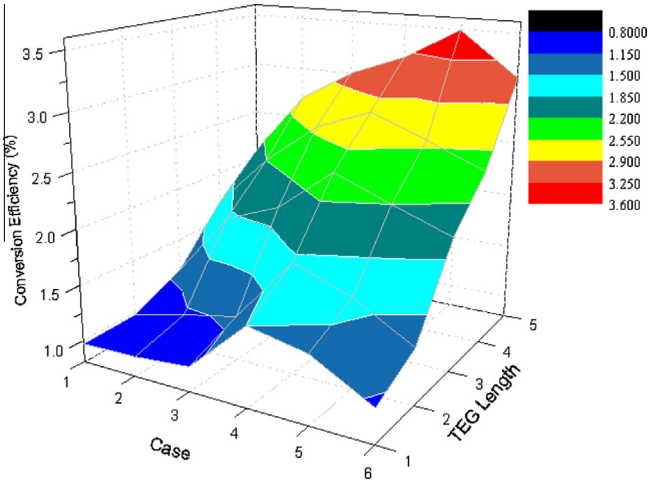

Fig. 15. Overall TEG efficiency vs. A_C for L_{ch1}–L_{ch5} at T_{in_cold} = 293 K, T_{in_hot} = 373 K and ΔP = 2 bar.

six TEG designs are therefore considered again, this time shortening L_{ch} but keeping the total system volume the same.

Fig. 13 shows the design from Fig. 3 where the TEG has been cut into L_{ch2} = 7.5 mm long sections along the length. The four sections are then placed next to each other, providing for a total width of 48 mm. The other five designs shortened (and widened) in the same fashion. As indicated in Table 3, the same designs are also cut into six sections of L_{ch3} = 5 mm and 12 sections of L_{ch4} = 2.5 mm and combined into correspondingly wider units with more channels.

Fig. 14(a) shows the power generation for each case with the different lengths and corresponding numbers of parallel channels. Shorter lengths and more parallel channels provide for a reduced flow resistance and a greater effective area for heat transfer near the inlet where the ΔT, and thus the thermoelectric conversion efficiency, is largest. For a given length, the total power goes through a maximum value determined by the competition between heat transfer area and flow nature as before. The reduced flow resistance is, however, also accompanied by an increase in the Reynolds number, i.e. there should be a tendency for the maximum to shift towards smaller channel heights. One more set of calculations is therefore performed in which the optimum channel length is identified for each of the six cases (Table 3). The results, included in Fig. 14(a), show a shift of the optimum to near Case 5 with an optimized L_{ch} as the corresponding *Re* increases from 422 to 1191 to 3533 (Fig. 14(b)), and the flow thus changes from laminar to turbulent, for this channel height (0.1875 mm). This should be near the true optimum design for the present operating conditions.

4.5. Overall TEG efficiency (η)

Fig. 15 shows the overall TEG efficiency η (the portion of energy that can be extracted from the liquid) with respect to A_C for all the lengths studied. Compared to Fig. 14(a), the more power generation associated with optimizing the TEG configuration, the higher η can be achieved. Case 5 in L_{ch5} shows the highest η of up to 3.5%. This should, however, only be considered as an ideal value, since several additional considerations need to be incorporated into the proposed thermoelectric model for further studies.

5. Conclusion

Two thermoelectric models are applied to assess the device performance of the TEGs, and the results show that the Coupled-field model performs better compared to the Simple model when validated using prior experiments [13]. The Coupled-field model is capable of representing the energy balance at the interface (TE effects) and the predicted power generation is within 8% error compared to the experiment validation. This is a much more improved result compared to most thermoelectric simulations available in the literature.

The simulations based on the Coupled-field model offers significant insight into the systematic effects of fluid heat exchanger design parameters on the efficiency of a generic thermoelectric generator (TEG). Not surprisingly, increasing the inlet temperature (T_{in_hot}) of the hot liquid leads to increases not only in the energy input, but also in the conversion efficiency with which this can be converted to electricity. Parallel flows of the hot and cold liquids lead to greater overall TEG efficiency as compared to counter flows. The pumping power required to maintain a pressure drop (ΔP) along the channels is significant, more than increasing the conversion capability, but can counteract the effect of a higher pressure drop on the net power.

In general, it is critical to maintain turbulent flow in channels. A larger number of channels at the micro scale provide for more interfaces with thermoelectric layers between them and smaller

temperature gradients across the channels, but eventually the increased flow resistance leads to a transition to laminar flow and lowers the power output, unless the pressure drop is raised. The power generation is therefore optimized by simultaneously minimizing channel dimensions (height and length) as much as possible without allowing (i) the flow to become laminar or (ii) significant thermal energy to exit out the other end of the channels.

It follows that further optimization may be achieved by introducing a stirred flow to mix the stream at low *Re*. Future work will also incorporate enhanced mixing using passive microstructures and high thermal conductivity nanofluids into the numerical model.

Acknowledgment

This work was supported by the Integrated Electronics Engineering Center at the State University of New York at Binghamton.

References

[1] L.E. Bell, Cooling, heating, generating power, and recovering waste heat with thermoelectric systems, Science 321 (2008) 1457–1461.
[2] S.B. Riffat, X.L. Ma, Thermoelectrics: a review of present and potential applications, Appl. Therm. Eng. 23 (2003) 913–935.
[3] A. Yadav, K.P. Pipe, M. Shtein, Fiber-based flexible thermoelectric power generation, J. Power Sources 175 (2008) 909–913.
[4] D.M. Rowe, G. Min, Evaluation of thermoelectric modules for power generation, J. Power Sources 73 (1998) 193–198.
[5] C. Wu, Analysis of waste-heat thermoelectric power generators, Appl. Therm. Eng. 16 (1996) 63–69.
[6] J.W. Stevens, Optimal design of small ΔT thermoelectric generation systems, Energy Convers. Manage. 42 (2001) 709–720.
[7] L.G. Chen, J.Z. Gong, F.R. Sun, C. Wu, Effect of heat transfer on the performance of thermoelectric generators, Int. J. Therm. Sci. 41 (2002) 95–99.
[8] J. Esarte, G. Min, D.M. Rowe, Modeling heat exchangers for thermoelectric generators, J. Power Sources 93 (2001) 72–76.
[9] D.T. Crane, G.S. Jackson, Optimization of cross flow heat exchangers for thermoelectric waste heat recovery, Energy Convers. Manage. 45 (2004) 1565–1582.
[10] R.O. Suzuki, D. Tanaka, Mathematical simulation of thermoelectric power generation with the multi-panels, J. Power Sources 122 (2003) 201–209.
[11] R.O. Suzuki, D. Tanaka, Mathematic simulation on thermoelectric power generation with cylindrical multi-tubes, J. Power Sources 124 (2003) 293–298.
[12] X.L. Gou, H. Xiao, S.W. Yang, Modeling, experimental study and optimization on low-temperature waste heat thermoelectric generator system, Appl. Energy 87 (2010) 3131–3136.
[13] B.T. Ismail, W.H. Ahmed, Thermoelectric power generation using waste-heat energy as an alternative green technology, Recent Patents Electr. Eng. 2 (1998) 27–39.
[14] Y.Y. Hsiao, W.C. Chang, S.L. Chen, A mathematic model of thermoelectric module with applications on waste heat recovery from automobile engine, Energy 35 (2010) 1447–1454.
[15] COMSOL 4.2 User Guide, COMSOL, Inc., Burlington, MA, 2012.
[16] X. Niu, J.L. Yu, Experimental study on low-temperature waste heat thermoelectric generator, J. Power Sources 188 (2009) 621–626.
[17] S.Y. Zhou, B.G. Sammakia, B. White, P. Borgesen, Thermoelectric systems modeling for conversion efficiency optimization, in: Proceeding of IEEE ITherm 2012 Conference, San Diego, CA, 2012, pp. 985–992.
[18] S.W. Angrist, Direct Energy Conversion, fourth ed., Allyn and Bacon, Inc., Boston, 1982. pp. 35–42.
[19] E.T. Topal, A flow induced vertical thermoelectric generator and its simulation using COMSOL multiphysics, in: Proceedings of the 2011 COMSOL Conference, Boston, MA, 2011.
[20] G. Mahan, B. Sales, J. Sharp, Thermoelectric materials: new approaches to an old problem, Phys. Today 50 (1997) 42.
[21] F.J. DiSalvo, Thermoelectric cooling and power generation, Science 285 (1999) 703–706.
[22] G. Chen, M.S. Dresselhaus, G. Dresselhaus, J.P. Fleurial, T. Caillat, Recent developments in thermoelectric materials, Int. Mater. Rev. 48 (2003) 45–66.
[23] D.G. Ebling, A. Jacquot, M. Jagle, H. Bottner, U. Kuhn, L. Kirste, Structure and thermoelectric properties of nanocomposite bismuth telluride prepared by melt spinning or by partially alloying with IV–VI compounds, Phys. Status Solid (RRL) 1 (2007) 238–240.